Dynamics of Light-Induced Conformational Changes of the Phoborhodopsin/Transducer Complex Formed in the *n*-Dodecyl β-D-Maltoside Micelle

Yukinori Taniguchi,[‡,⊥] Tatsuya Ikehara,[‡] Naoki Kamo,[§] Hiroshi Yamasaki,[‡] and Yoshinori Toyoshima*[,‡]

Nano-biotechnology Research Center and Department of Bioscience, School of Science and Technology, Kwansei Gakuin University, Sanda, Hyogo, Japan, and Faculty of Advanced Life Sciences, Hokkaido University, Sapporo, Hokkaido, Japan

Received December 2, 2006; Revised Manuscript Received February 28, 2007

ABSTRACT: A complex of photoreceptor phoborhodopsin (*p*pR; also called sensory rhodopsin II) and its cognate halobacterial transducer II (*p*HtrII) existing in the plasma membrane mediates the light signal to the cytoplasm in the earliest step of negative phototaxis in *Natronomonas pharaonis*. We have investigated the dynamics of the light-induced conformational changes of the *p*pR/*p*HtrII(1−159) complex formed in the presence of 0.1% *n*-dodecyl β-D-maltoside (DDM) by a fluorescence resonance energy transfer (FRET) based method. Fluorescence donor and acceptor dyes were linked to cysteine residues genetically introduced at given positions in *p*HtrII and *p*pR. The light-induced FRET efficiency changes for various pairs of dye-labeled cysteine residues were determined to examine dynamics of movements of given residues in the transmembrane and the linker region including the HAMP domain in *p*HtrII induced by photoexcitation of *p*pR. Upon flash excitation of *p*pR, FRET efficiency changed depending on pairs of the labeled cysteine residues. The distances between V185 in *p*pR and the five given residues (102 through 141) in the *p*HtrII linker region estimated from the FRET efficiency increased by 0.3−0.8 Å; on the other hand, the distances between S31 in *p*pR and the five residues in *p*HtrII decreased. The changes arose within 70 ms (the dead time of instrument) and decayed at a rate of 1.1 ± 0.2 s. Azide significantly increased the decay rate of light-induced FRET efficiency changes by accelerating the decay of the M state of *p*pR. The decay rate of FRET efficiency changes coincided with the rate of recovery of the *p*pR to the initial state but not the decay of the M state. We conclude that the light-induced conformational change of *p*HtrII occurs before, at the formation or during the M state, and its relaxation is coupled tightly with the decay of the O state of *p*pR in the 1:1 complex formed in the DDM micelle.

Phoborhodopsin (*p*pR;[1] also called *pharaonis* sensory rhodopsin II, NpSRII) is a photoreceptor protein of negative phototaxis in *Natronomonas pharaonis*. The *p*pR and its cognate transducer (*Halobacterium* transducer II; *p*HtrII) form a 2:2 complex in which the *p*HtrII dimer is sandwiched between two *p*pR molecules in the plasma membrane (*1*, *2*). The *p*HtrII is a homologue of the chemotaxis receptor (methyl-accepting chemotaxis protein: MCP) of *Escherichia coli* and is thought to be accommodated with a histidine kinase CheA and adaptor protein CheW in the cytoplasmic region. The *p*pR/*p*HtrII complex mediates the light signal to the cytoplasmic signal transduction pathway in the earliest step of phototaxis. The structure of the transmembrane region of the complex was determined by X-ray crystallography with atomic resolution (*2*, *3*). The cytoplasmic region of *p*HtrII has been thought to form a four-helical-bundle coiled-coil structure similar to chemoreceptors (*4*, *5*). The structure of the *p*HtrII linker region, which connects the transmembrane and cytoplasmic regions, has been investigated by NMR (*6*, *7*), EPR (*8*, *9*), and tryptophan FRET (*10*) but not determined crystallographically. The *p*HtrII linker region contains the HAMP domain, of which structure and function in the signal transduction process were recently suggested in *Archaeoglobus fulgidus* by NMR (*11*).

The dynamics of *p*pR photointermediates (states) has been well investigated. Photoexcitation of *p*pR induces a cyclic conformational change (photocycle), in which K, L, M, and O intermediate states named in the order of their appearance were identified (*12*−*14*). On the other hand, the conformational change of *p*HtrII in the *p*pR/*p*HtrII complex induced by illumination of *p*pR has less information; Klare et al. showed a rotation of transmembrane helix 2 (TM2) of *p*HtrII, which was induced by the outward tilt of helix F of *p*pR, during the M (M_2) state of *p*pR (*1*, *15*), and Yang et al. showed that the membrane proximal region of *p*HtrII became close to the E−F loop of *p*pR when it was photoexcited (*10*). These conformational changes are thought to occur without secondary structure change, suggesting rigid-body motion of the complex (*16*). However, conformational changes of the linker region and the cytoplasmic region of *p*HtrII during state change in *p*pR have never been detected directly, although a rotation of the HAMP domain in the linker region was suggested (*11*). Since the M state has the longest lifetime in the photocycle of *p*pR and large conformational change is induced during the M state in the case of bacteriorhodopsin

* To whom correspondence should be addressed. Tel/Fax: 81-72-461-4874. E-mail: ytoyoshima@rinku.zaq.ne.jp.

‡ Kwansei Gakuin University.

§ Hokkaido University.

⊥ Present address: School of Materials Science, Japan Advanced Institute of Science and Technology, Nomi, Ishikawa, Japan.

[1] Abbreviations: *p*pR, *pharaonis* phoborhodopsin; *p*HtrII, *pharaonis* halobacterial transducer II; FRET, fluorescence resonance energy transfer; DDM, *n*-dodecyl β-D-maltoside; TM, transmembrane; EPR, electron paramagnetic resonance.

10.1021/bi602482s CCC: $37.00
Published on Web 04/14/2007

(reviewed in ref *17*), it has been thought that the M state is the most crucial state in the signaling process of *p*pR (signaling state). Recently, Sudo and Spudich showed that bacteriorhodopsin modified with only three amino acid mutations in its membrane-embedded domain mediates phototaxis signals through the *p*HtrII genetically expressed in the *Halobacterium salinarum* strain which lacks the four native rhodopsins (bacteriorhodopsin, halorhodopsin, sensory rhodopsin I, and phoborhodopsin) and the two transducer proteins (HtrI and HtrII) (*18*), implying that the conformational change that occurs in the pumping cycle of bacteriorhodopsin shares signal-producing features with that of *p*pR. In the case of *p*pR, Spudich and colleagues concluded from experiments using retinal analogues that both M and O states are signaling states (*19*). On the other hand, studies using a laser flash photolysis and transient grating method indicated that the dynamics of volume expansion and contraction of the *p*pR/*p*HtrII complex coincided with the rise and decay of the O state, respectively, suggesting that the O state is the signaling state (*20*). EPR study indicated that the relaxation of rotation of TM2 in *p*HtrII was slower than the whole process of the photocycle of *p*pR, suggesting that conformational change of *p*HtrII is uncoupled from the state changes of the *p*pR during the last step of the photocycle (*1*). Thus, the previous results concerning dynamics of the conformational change of the complex are controversial.

Recently, we employed a fluorescence resonance energy transfer (FRET) based method, which provides a convenient spectroscopic method to study the dynamics of the structural change of the protein complex, to investigate light-induced conformational changes of the *p*pR/*p*HtrII complex (*21*). In the application of FRET to the *p*pR/*p*HtrII system, spectral overlap of the dyes with the absorption of the intermediates of *p*pR per se had been thought to prevent a quantitative analysis. This problem was solved by using recently developed far-red fluorescent dyes, Cy5 and Alexa660 as fluorescent donors and Cy7Q, HiLyte Fluor 750 (HF750), and DY750 as acceptors. Subangstrom-scale changes of distances from V185 in *p*pR to V78, A79, and D102 in *p*HtrII were successfully detected using the pair Alexa660 and Cy7Q. In this study, we have investigated the dynamics of the light-induced movement of several residues in the *p*HtrII (A80, D102, E110, L120, S130, and A141; see Figure 1) relative to S31, V58, and V185 in *p*pR and intramolecular movement of A80 against L120 in *p*HtrII in the *p*pR/*p*HtrII complex formed in 0.1% DDM and the effect of azide on the dynamics. The results of FRET experiments suggest that the light-induced conformational change of *p*HtrII occurs before, at the formation, or during the M state, and its relaxation takes place concomitantly with the decay of the O state of *p*pR but not the M state.

MATERIALS AND METHODS

Reagents. The thiol reactive dye Alexa660 C_2-maleimide was purchased from Invitrogen Corp. (Carisbad, CA). Cy5-maleimide and Cy7Q-maleimide were from GE Healthcare Bio-Sciences Corp. (Piscataway, NJ). The detergents *n*-dodecyl β-D-maltoside (DDM) and *n*-octyl β-glucoside (OG) were from Dojindo Laboratories (Kumamoto, Japan). All-*trans*-retinal and isopropyl 1-thio-β-D-galactopyranoside (IPTG) were from Wako Pure Chemical Industries, Ltd. (Osaka, Japan).

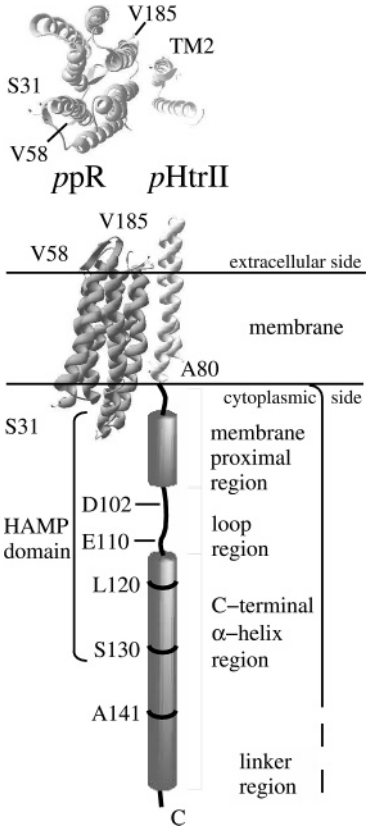

FIGURE 1: Scheme of positions for single-cysteine substitution in *p*pR and *p*HtrII examined in this study. The top is a view from the cytoplasmic side. The ribbons represent the crystal structure of the complex (PDB code 1H2S). The cylinders and the lines in the *p*HtrII linker region were predicted α-helix and extended (loop) regions, respectively.

Construction of Plasmids. Expression plasmids of *p*pR and *p*HtrII(1−159) possessing a 6× histidine tag at the C terminus were constructed previously (*22*), where *p*HtrII-(1−159) stands for truncated *p*HtrII protein expressed from the 1st to 159th residue instead of the whole length. Expression plasmids for *p*pR and *p*HtrII(1−159) with single cysteine substitution at various positions were prepared by PCR using the QuikChange method. Introduction of the single mutation was confirmed by sequence analysis using an automated sequencer, PRISM 3100-Avant, and a BigDye Terminator v3.1 cycle sequencing kit (Applied Biosystems).

Protein Expression, Purification, and Fluorescent Labeling. Wild-type and mutant proteins of *p*pR and *p*HtrII(1−159) were expressed in *E. coli* BL21(DE3) cultured in 2× YT medium by IPTG (1 mM) induction (*23*). Purification of each protein was performed with Ni-NTA agarose (Qiagen) and DEAE-Sephacel (GE Healthcare) columns as described previously (*21*). The purities of the *p*pR and *p*HtrII were checked by SDS−PAGE and, further, the ratio of absorbance at 500 nm to that at 280 nm in the case of *p*pR. SDS−PAGE of the purified *p*pR and *p*HtrII showed a single band corresponding to 25 and 17 kDa, respectively (see Figure 2A). Purified *p*HtrII and *p*pR were labeled with donor (Alexa660-maleimide) and acceptor (Cy7Q-maleimide) on their genetically introduced cysteine residue, respectively (*21*). The concentrations of *p*pR and dyes were determined by measuring their absorbance, and that of *p*HtrII was done by using the Micro BCA protein assay kit (Pierce). Labeling efficiency was calculated from their concentrations for each

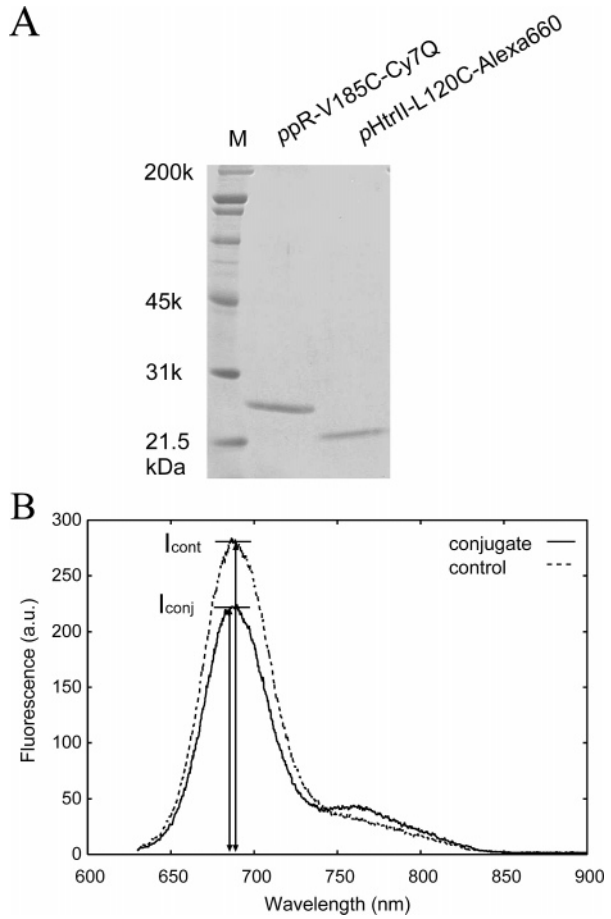

FIGURE 2: (A) SDS−PAGE analysis of dye-labeled protein. Three micrograms of each protein was loaded on 15% polyacrylamide gels. Labeling efficiencies for *p*pR-V185C-Cy7Q and *p*HtrII-L120C-Alexa660 were 0.45 and 0.51, respectively. Expected molecular masses of *p*pR and *p*HtrII proteins are 25 and 17 kDa, respectively, and those of Cy7Q and Alexa660 are 1.1 and 0.9 kDa, respectively. (B) Fluorescence spectra of the *p*pR-V185C-Cy7Q/*p*HtrII-L120C-Alexa660 complex (conjugate, solid line) and the nonlabeled *p*pR-V185C/*p*HtrII-L120C-Alexa660 complex and free Cy7Q at their corresponding concentrations (control, dotted line). The concentration of *p*pR and *p*HtrII was 8 and 4 μM, respectively. The excitation wavelength was 610 nm.

sample preparation. The labeling efficiencies of acceptor to *p*pR-S31C, -V58C, and -V185C were 0.37−0.58, 0.86, and 0.68−0.91, respectively, and those of donor to *p*HtrII-A80C, -D102C, -E110C, -L120C, -S130C, and -A141C were 0.25−0.28, 0.48−0.53, 0.51−0.70, 0.38−0.59, 0.38−0.57, and 0.57, respectively. For double labeling of *p*HtrII using A80C and L120C by the donor and acceptor dyes, the protein was incubated with 3-fold Alexa660-maleimide and 6-fold Cy7Q-maleimide for 2 h at room temperature. Their labeling efficiencies were 0.30 and 0.71, respectively. This sample should be a mixture of nonlabeled, differently single-labeled, and double-labeled *p*HtrII. However, among them, only *p*HtrII with $A80_{donor}-L120_{acceptor}$ or $A80_{acceptor}-L120_{donor}$ are expected to exhibit the flash-induced change in FRET efficiency. No degradation of the proteins during the dye-labeling process was confirmed as shown in Figure 2A.

Measurement of FRET Efficiency. The procedure for measurement of FRET efficiency and analysis of the data were done as described previously (*21*). Prior to the fluorescence measurements, samples were incubated in buffer M (50 mM HEPES, pH 7.0, 400 mM NaCl, 0.1% DDM) for at least 3 h to form the complex. To obtain FRET efficiency, the effect of absorption of the fluorescence emitted from the donor by the acceptor was eliminated as follows. The fluorescence spectrum in a solution of the *p*pR-acceptor/*p*HtrII-donor complex (conjugate) was measured concomitantly with that in a solution containing the nonlabeled *p*pR/*p*HtrII-donor complex and free acceptor (control) at their corresponding concentrations, as shown in Figure 2B. The FRET efficiency was determined by analyzing the spectra illustrated in Figure 2B by the equation:

$$E = \frac{1}{\gamma}\left(\frac{I_{cont} - I_{conj}}{I_{cont}}\right) \quad (1)$$

where γ is a labeling efficiency of acceptor and I_{conj} and I_{cont} are the fluorescence intensities at the peaks in the spectra of the conjugate and control samples. The FRET-derived distances and their changes were calculated under the assumption that FRET does not occur in the control because the average distance between the donor and the bulk acceptor is sufficiently long compared to the Förster distance.

Time-Resolved FRET Measurement. Transient changes of fluorescent intensity upon photoexcitation of *p*pR were measured with a fluorescence spectrometer associated with a flash apparatus and analyzed as previously described in ref *21*. For the measurements in the presence of azide, the electronic low-pass filter (cutoff frequency: 100 Hz) was removed to reduce the dead time of the instrument. To avoid the presence of labeled *p*HtrII which is not associated with labeled *p*pR, 8 μM labeled *p*pR and 4 μM labeled *p*HtrII were incubated in buffer M for at least 3 h at room temperature and submitted to the fluorescent measurement. All measurements were carried out at 20 °C, and data were obtained as an average of 160 flash measurements. Apparent FRET efficiency at time *t*, $E_{app}(t)$, was calculated from the fluorescence intensities of the conjugate and control samples at 690 nm (*21*). The distance change [$\Delta R(t)$] was obtained by using the formula:

$$\frac{\Delta R(t)}{R} = -\frac{1}{\psi}\left(\frac{\Delta E_{app}(t)}{6E(1-E)}\right) \quad (2)$$

assuming $\Delta R(t) \ll R$. Here, E is the FRET efficiency at the initial state, $\Delta E_{app}(t)$ [$=E_{app}(t) - E$] is apparent FRET efficiency change at time *t*, and ψ is the excitation efficiency of *p*pR upon the flash, which is dependent on the arrangement of the apparatus. The value of ψ in each experiment was determined from the relative reduction of the *p*pR initial state upon the flash obtained by measuring the absorbance change at 500 nm. The values were 0.34−0.52 among all measurements.

Transient ppR Absorbance Change Measurements. The apparatus for measurement of transient absorbance changes during the photocycle was essentially the same as that of the transient fluorescence measurement except for the source of measuring light. An I_2 lamp was used as the source, and a band path filter (Toshiba, KL40, KL50, or KL56) was placed in front of the cell. The intensity of transmitted light was recorded for each wavelength in the absence of the SC64 filter. To avoid the presence of *p*pR, which is not associated with *p*HtrII, 4 μM *p*pR was incubated with 16 μM *p*HtrII in buffer M for at least 3 h at room temperature (*24*). All

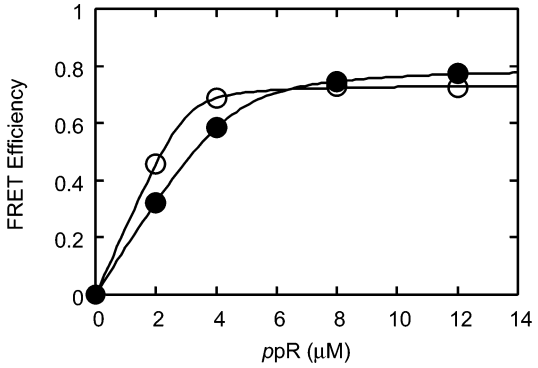

FIGURE 3: FRET efficiencies at various concentrations of *p*pR-V185C under a fixed *p*HtrII-A79C (open circles) or *p*HtrII-D102C (closed circles) concentration of 4 μM. Cy5 and Cy7Q were utilized as the fluorescence donor and acceptor, respectively.

measurements were performed at 20 °C, and the data were obtained as an average of 16 flash measurements. The least-squares curve fitting analysis was performed using Gnuplot software as described previously (*12*). The time-dependent absorbance changes of the M, O, and initial state of *p*pR were given as

$$\Delta A_{\mathrm{M}} = A_1 \exp(-k_1 t)$$

$$\Delta A_{\mathrm{O}} = A_2 \frac{k_1}{k_2 - k_1}[\exp(-k_1 t) - \exp(-k_2 t)]$$

$$\Delta A_{\mathrm{I}} = A_3 \frac{1}{k_2 - k_1}[k_1 \exp(-k_2 t) - k_2 \exp(-k_1 t)] \quad (3)$$

respectively, where k_1 and k_2 are decay rates of the M and O states and A_1, A_2, and A_3 are constants depending on the measuring wavelength, respectively. The observable absorbance changes at 400, 500, and 560 nm are given by

$$\Delta A_{400} = \Delta A_{\mathrm{M}} + \alpha_1 \Delta A_{\mathrm{O}} + \alpha_2 \Delta A_{\mathrm{I}}$$

$$\Delta A_{560} = \alpha_3 \Delta A_{\mathrm{M}} + \Delta A_{\mathrm{O}} + \alpha_4 \Delta A_{\mathrm{I}}$$

$$\Delta A_{500} = \alpha_5 \Delta A_{\mathrm{M}} + \alpha_6 \Delta A_{\mathrm{O}} + \Delta A_{\mathrm{I}} \quad (4)$$

where $\alpha_1 - \alpha_6$ represent the contribution of spectral overlap of these states at their wavelengths. The kinetic data at 400, 500, and 560 nm were analyzed by combining eqs 3 and 4.

RESULTS AND DISCUSSION

Conformation in the pHtrII Linker Region in the ppR/pHtrII Complex Formed in DDM. The FRET-derived dye to dye distances between each of several residues in the *p*HtrII linker region (D102, E110, L120, S130, and A141) and each of three residues in *p*pR (S31, V58, and V185) in the initial state complex were measured. Here, S31 and V58 are located in the cytoplasmic side and extracellular side of the helix B, respectively, and V185 is located in the extracellular F−G loop (see Figure 1). As illustrated in Figure 3 for the pairs *p*pR-V185C-Cy7Q/*p*HtrII-A79C-Cy5 and *p*pR-V185C-Cy7Q/*p*HtrII-D102C-Cy5, when the concentration of the *p*pR-acceptor in the solution was increased (0−12 μM) at a fixed concentration of the *p*HtrII-donor (4 μM), FRET efficiency increased with an increase of *p*pR-acceptor concentration and saturated at 4 μM, suggesting that *p*pR and *p*HtrII form a complex with a 1:1 ratio in 0.1% DDM. These results are consistent with previous results obtained in detergent solution in which a 1:1 *p*pR/*p*HtrII heterodimer complex (1:1 complex) was found to form (*1*, *9*, *24*, *25*). On the basis of these results, FRET efficiency and its change were measured with the solutions containing 8 μM *p*pR and 4 μM *p*HtrII and analyzed under the assumption of the complete formation of the 1:1 complex. The distances derived from FRET efficiency are summarized in Table 1.

It is evident that FRET-derived distances are different from the corresponding amino acid distance (C_α distance) estimated from the crystal structure because of the bulkiness, orientation, and mobility of the dyes and the microenvironment separating the donor and acceptor dyes, such as the refractive index of the medium. For example, the FRET-derived distances from A80 in *p*HtrII to S31 (located in cytoplasmic side), V58 (extracellular side), and V185 (extracellular side) in *p*pR were 67, 60, and 56 Å, respectively, which were considerably longer than that of the corresponding amino acid distance in the crystal, 30, 34, and 29 Å, respectively (*2*). Furthermore, the FRET distance between A80 in *p*HtrII and S31 in *p*pR was longer than that between A80 in *p*HtrII and V58 in *p*pR, while the amino acid distance between A80 and S31 was shorter than that between A80 and V58 in the crystal (*2*). This discrepancy may be explained by considering the effect of the refractive index (n) of the medium separating the donor and acceptor dyes: if we assume $n = 1.33$ (water) for *p*pR-S31/*p*HtrII-A80 and $n = 1.45$ (1.4 for lipid and 1.5 for protein) for *p*pR-V58/*p*HtrII-A80, the Förster distance R_0^6 for the former becames larger by a factor of 1.41 than that for the latter because R_0^6 is inversely proportional to n^4 (*26*). When the environment of the dyes is substantially equivalent as in the case of the *p*pR-V58/*p*HtrII-A80 and *p*pR-V185/*p*HtrII-A80 pairs, the difference between the FRET-derived distance for the *p*pR-V58/*p*HtrII-A80 pair and that for the *p*pR-V185/*p*HtrII-A80 pair (5 Å) was consistent with the corresponding value determined in crystal (4 Å), suggesting that the FRET-derived distance well reflects the amino acid distance. Since S31 in *p*pR and the residues in the HAMP domain of *p*HtrII are located in the aqueous environment on the cytoplasmic side, the FRET-derived distances from S31 in *p*pR to these residues in *p*HtrII may be compared without this environmental effect. The FRET-derived distances from S31 in *p*pR to D102 or E110, in the putative loop region of the *p*HtrII linker, were not so different from that between S31 in *p*pR and A80 in the transmembrane region of *p*HtrII, suggesting that the loop region is located in the vicinity of *p*pR. These results are consistent with the previous EPR-based structural model of the *p*HtrII membrane proximal region (83−101), in which the region interacts with the E−F loop of *p*pR, in the detergent solution (*9*). The FRET-derived distances from S31 or V185 in *p*pR to L120, S130, or A141 in the second α-helix region in the *p*HtrII linker (*6*−*8*, *10*) increased toward the C terminus in the *p*HtrII linker, suggesting a rod-like structure of the region, which elongates to a direction going away from *p*pR. This aspect of the *p*HtrII linker region in the complex formed in the presence of DDM does not agree with the solution structure of the HAMP domain fragment in the absence of detergent, in which helixes of two HAMP domain fragments were suggested to interact with each other and form the homodimeric, parallel four-helical coiled-coil

Table 1: Quantum Yield (QY) of *p*HtrII-Alexa660 and Förster Distance (R_0), FRET Efficiency (E), FRET-Derived Distance (R), and Change of the Distance (ΔR) by Flash Excitation of *pp*R[a]

		transmembrane	linker				
	*p*HtrII	A80	D102	E110	L120	S130	A141
	QY	0.29	0.34	0.29	0.26	0.30	0.28
	R_0 (Å)	61	64	64	61	63	63
*pp*R V185	E[b]	0.61 ± 0.05	0.54 ± 0.03[e]	0.47 ± 0.05	0.45 ± 0.11	0.37 ± 0.01	0.31 ± 0.04
	R (Å)[c]	56 ± 1.9	63 ± 1.4[e]	65 ± 2.3	63 ± 4.7	69 ± 0.5	73 ± 2.2
	ΔR (Å)[d]	−1.3 ± 0.07	0.33 ± 0.1[e]	0.54 ± 0.22	0.77 ± 0.06	0.45 ± 0.04	0.32 ± 0.02
S31	E[b]	0.36 ± 0.002	0.36 ± 0.005	0.34 ± 0.002	0.23 ± 0.03	0.20 ± 0.002	0.17 ± 0.01
	R (Å)[c]	67 ± 0.1	71 ± 0.2	71 ± 0.08	75 ± 1.7	80 ± 0.2	82 ± 1.0
	ΔR (Å)[d]	−0.67 ± 0.08	−1.8 ± 0.3	−1.3 ± 0.59	−0.61 ± 0.32	ND	ND
V58	E[b]	0.52 ± 0.03	0.38 ± 0.02		0.10 ± 0.01		
	R (Å)[c]	60 ± 1.0	70 ± 0.6		88 ± 1.3		
	ΔR (Å)[d]	1.2 ± 0.4	0.36 ± 0.03		ND		

[a] Data represent the mean ± SD of two individual experiments. The residues in *pp*R were labeled with Cy7Q, and those in *p*HtrII were labeled with Alexa660. ND = not detected. [b] FRET efficiencies were calculated using eq 1. [c] FRET-derived distances were calculated using $E = R_0^6/(R_0^6 + R^6)$ under the assumption of isotropic orientation of dyes, i.e., $\kappa^2 = {}^2/_3$, and the refractive index used in calculation of the Förster distance R_0 was 1.4 (*26*). [d] FRET-derived distance changes upon flash excitation of *pp*R were calculated using eq 2. [e] Taniguchi et al. (*21*).

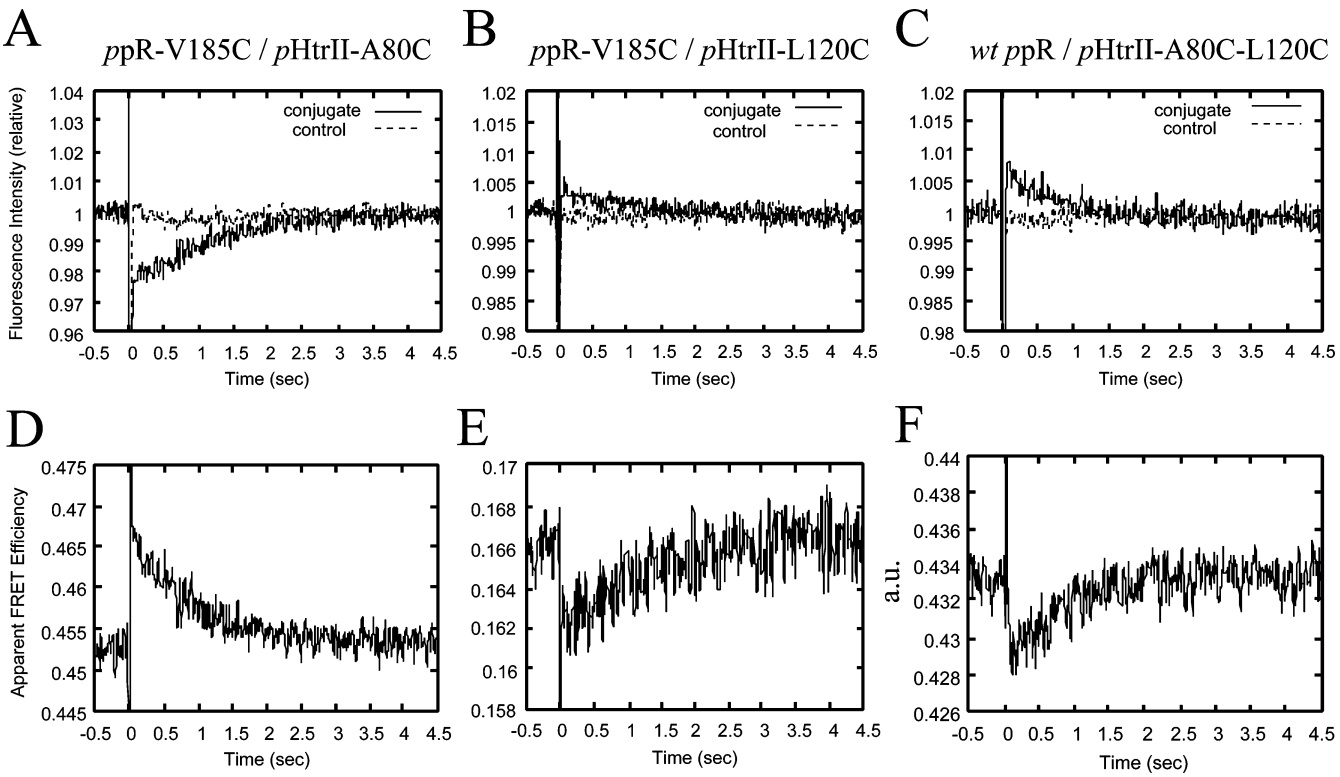

FIGURE 4: Change of FRET efficiency upon a flash excitation of *pp*R. (A−C) Changes of fluorescence intensity of the conjugate and control samples of *pp*R-V185C/*p*HtrII-A80C (A), *pp*R-V185C/*p*HtrII-L120C (B), and wt *pp*R/*p*HtrII-A80C-L120C (C). The excitation wavelength was 633 nm (He−Ne laser). Fluorescence was monitored at the wavelength giving the maximum of the donor fluorescence (690 nm). Each trace was an average of 160 flash data recorded at 20 °C. The very sharp decrease and recovery within 70 ms was an instrumental artifact. The concentrations of *pp*R and *p*HtrII were 8 and 4 μM, respectively. (D−F) Change of apparent FRET efficiency upon a flash excitation of *pp*R in *pp*R-V185C/*p*HtrII-A80C (D), *pp*R-V185C/*p*HtrII-L120C (E), and wt *pp*R/*p*HtrII-A80C-L120C (F). FRET efficiency was calculated from the data shown in (A) and (B) without correction of labeling efficiency and excitation yield of *pp*R. In the case of *pp*R/*p*HtrII-A80C-L120C (F), the sample was a mixture of nonlabeled, differently single-labeled, and double-labeled *p*HtrII. However, among them, only *p*HtrII with $A80_{donor}-L120_{acceptor}$ or $A80_{acceptor}-L120_{donor}$ are expected to exhibit the flash-induced change in FRET efficiency.

structure by NMR (*11*). This discrepancy may be due to the absence of *p*HtrII−*p*HtrII dimerization in the 1:1 *pp*R/*p*HtrII complex and looseness of the hydrophobic interaction between two helixes in a HAMP domain fragment by the presence of detergent.

Conformational Change of the Complex upon Flash Excitation of ppR. Flash-induced changes in the FRET-derived distances were investigated for various pairs of the *pp*R and *p*HtrII residues (Figure 4, Table 1). Upon a flash excitation of *pp*R, the FRET efficiency of the *pp*R-V185C-Cy7Q/*p*HtrII-A80C-Alaxa660 pair initially increased within 70 ms (dead time of the instrument) and relaxed with a rate of 1.1 ± 0.02 s to the level of the initial state (Figure 4B). In the case of the *pp*R-V185C/*p*HtrII-L120C pair, on the other hand, the FRET efficiency initially decreased (Figure 4D). Thus, the difference in direction and magnitude of the FRET efficiency changes induced by a flash excitation of *pp*R was observed among the pair of residues examined. An

intramolecular flash-induced distance change was also observed between A80 and L120 in *p*HtrII labeled with Alexa660 and Cy7Q. As shown in Figure 4F, the FRET efficiency of *p*pR/*p*HtrII-A80-L120-Alexa660-Cy7Q decreased within 70 ms and relaxed at similar rate, 1.0 ± 0.11 s. Distance changes at various pairs of residues calculated from the FRET efficiency changes after correction of labeling efficiency and flash yield are summarized in Table 1.

The positions of V58 and V185 in *p*pR scarcely change from the initial (unphotolyzed) at the M state in the crystal at low temperature (*3*). If we assume that these residues do not move in detergent solution at room temperature, Table 1 indicates that, upon illumination of *p*pR, the residues in the linker region (D102, E110, L120, S130, and A141) move away from both V58 and V185 in *p*pR, located at the extracellular surface, by 0.3−0.7 Å. The simplest suggestion is as follows: Conformational changes occur in the α-helix of the membrane proximal or C-terminal α-helix region where the tight α-helix becomes slightly loose so as to increase the distance. However, the change of 0.3−0.7 Å seems too small by this suggestion, because the length per one pitch of the α-helix is 5.4 Å. Another possibility might be a rotation of these regions as pointed out by Klare et al. (*1*, *15*). However, from the present data, we cannot infer whether the rotation occurs or not. The other possibility to be considered is the interaction between the E−F loop in *p*pR and the membrane proximal region pointed out by Yang et al., suggesting that the membrane proximal region of *p*HtrII become close to the E−F loop of *p*pR when it was photoexcited (*10*). Neither we can infer the validity of this possibility: Lateral (i.e., along with membrane) movement of the membrane proximal region of *p*HtrII is difficult to detect as a change of distance from V58 or V185 in *p*pR, and the decrease of the FRET-derived distance from S31 in *p*pR to the residues in the linker region of *p*HtrII (D102, E110, and L120) does not necessarily indicate that these residues of *p*HtrII move to *p*pR, because S31 in *p*pR is reported to move toward helix A by 0.7 Å in the crystal (*3*). Then, the interpretation of the present data is difficult. It should be mentioned, however, that the photoinduced changes in distances from V185 of *p*pR to A80 and to the residues in the linker region are in opposite directions, suggesting that the conformational changes in the linker region might be different from that of the transmembrane region.

Thus, from the data obtained here, we cannot draw a possible model of the conformational change, but it should be worth noting that the present report reveals the occurrence of the conformational change in the HAMP domain when *p*pR, a receptor, is stimulated.

Coupling of Conformational Changes of pHtrII and ppR. As shown in Figure 4, all of the FRET efficiency changes observed in several pairs of the residues in *p*pR and *p*HtrII including an intramolecular residual movement in *p*HtrII arose within the dead time of the instrument (70 ms) and decayed at a rate of 1.1 ± 0.2 s upon flash-light excitation of *p*pR, suggesting that it occurred before or at the formation of the M state and relaxed concomitantly with the decay of the M state or that of the O state. To clarify the coupling process between *p*HtrII and *p*pR in the relaxation of the light-induced conformation, we investigated the effect of azide on the decay rate of the flash-induced FRET efficiency change and compared them with the rates of the state change of *p*pR in the absence and presence of azide. Azide has been known to facilitate transfer of the proton to the deprotonated Schiff base in the M state and accelerate the decay of the M state of *p*pR in detergent solution (*27*) and in the lipid membrane (*28*), both in the absence of *p*HtrII. At first, we investigated the dynamics of the photocycle in the *p*pR/*p*HtrII complex formed in 0.1% DDM and the effect of azide on the rates of the photocycle. In the absence of azide, the decay rates of M and O states in the *p*pR/*p*HtrII complex were 0.73 and 8.8 s^{-1}, respectively (Figure 5A). The addition of 100 mM azide accerelated the M decay by about 50-fold (Figure 5B), which is consistent with the report by Sudo et al. (*29*). The decay rate of the O state in the presence of 100 mM azide was 8.4 s^{-1}, which was almost the same as that in the absence of azide, 8.8 s^{-1}. Figure 6A shows the effect of azide on the decay process of the flash-induced FRET efficiency change in the *p*pR/*p*HtrII 1:1 complex. The decay rate increased with increasing concentration of azide, suggesting that the conformational change of the *p*HtrII is tightly coupled with that of *p*pR in the photocycle. The decay coincided with the recovery of *p*pR to the initial state but not the decay of the M state in the absence and presence of azide (Figure 6B,C). Essentially the same results were

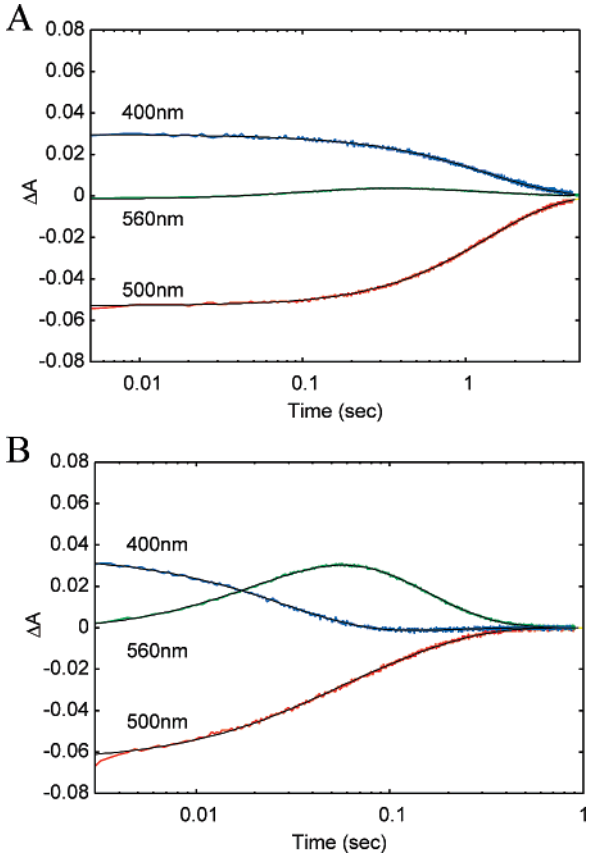

FIGURE 5: Photocycle of *p*pR in the 1:1 *p*pR/*p*HtrII complex formed in 0.1% DDM solution. (A, B) Flash-induced absorbance changes of *p*pR-V185C/*p*HtrII-L120C in the absence (A) and presence (B) of 100 mM azide. Absorbance changes measured at 400 nm (mainly M state), 500 nm (initial state), and 560 nm (O state) were shown. The regression curves obtained by least-squares curve fitting analysis (eq 4) were indicated as black lines. The decay rates of M and O states were 0.73 and 8.8 s^{-1} in the absence and 34 and 8.4 s^{-1} in the presence of azide, respectively. The concentration of *p*pR-V185C and *p*HtrII-L120C was 4 and 16 μM, respectively.

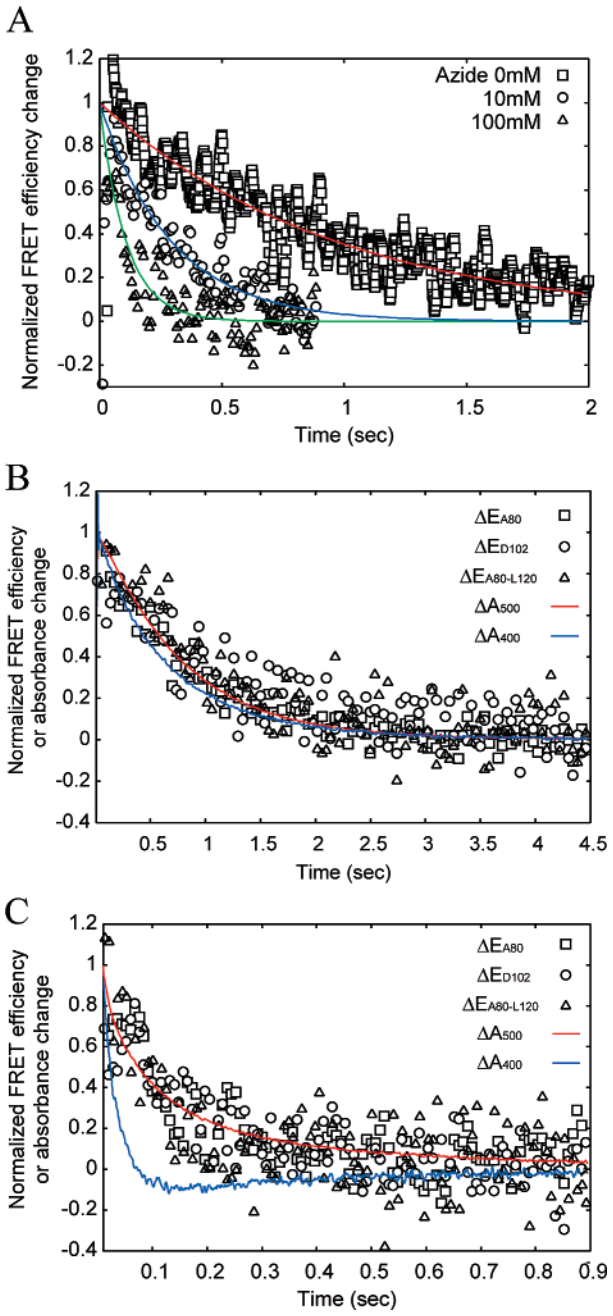

FIGURE 6: Dynamics of the relaxation process of light-induced motion between the indicated residues in the 1:1 *p*pR/*p*HtrII complex formed in 0.1% DDM solution. (A) Relaxation of FRET efficiency to the initial level in the presence of the indicated concentrations of azide. FRET efficiency change was measured in the *p*pR-V185C-Cy7Q/*p*HtrII-A80C-Alexa660 pair. The solid lines were single exponential curves obtained by a least-squares curve fitting procedure. (B, C) FRET efficiency change overlaid on absorbance changes at 400 nm (blue) and 500 nm (red) in the absence (B) and presence of 100 mM azide (C). FRET efficiency changes were measured in the *p*pR-V185C-Cy7Q/*p*HtrII-A80C-Alexa660 (squares), *p*pR-V185C-Cy7Q/*p*HtrII-D102C-Alexa660 (circles), and wt *p*pR/*p*HtrII-A80C-L120C-Alexa660-Cy7Q (triangles) pairs.

obtained in the transmembrane region (*p*HtrII-A80C), linker region (*p*HtrII-D102C), and intramolecular (*p*HtrII-A80C-L120C) movements. These results indicated that the relaxation of the light-induced conformation of *p*HtrII to the initial state was tightly coupled with the decay of the O state of *p*pR.

Sudo et al. estimated the dissociation constant between *p*pR and *p*HtrII at the ground, M, and O states to be 0.16 μM (*30*), 15 μM (*24*), and 0.15 μM (*31*), respectively. Combining these values with the present results, we can suppose as follows: before M or at the M formation, the signal transfers from the receptor *p*pR to *p*HtrII, and then the interaction between them becomes weak by a factor of 100. At the O state, they rebind strongly, and the change in *p*pR from O to the original state and the return of the *p*HtrII conformation to the original dark state are tightly coupled with each other in the *p*pR/*p*HtrII complex. It should be mentioned that the decay rate of the O state in the *p*pR/*p*HtrII complex increased by 6-fold compared with that in the absence of *p*HtrII, 1.5 s^{-1} (data not shown), suggesting that the relaxation of the O state of *p*pR is accelerated by the formation of the complex with *p*HtrII as to be coupled with the conformational change of *p*HtrII. The same behaviors were obtained previously in 0.1% DDM solution for the O-like state, which was measured in the M state-lacking mutant, *p*pR-D75N (*31*).

Previously, it has been shown with FTIR that the hydrogen bond between Y199 in *p*pR and N74 in *p*HtrII re-formed concomitantly with the decay of the M and/or O states in the lipid membrane (*32*). A study using the transient grating method has shown that the rates of the volume expansion and contraction, which may reflect conformational change, took place concomitantly with the rise and decay of the O state, respectively, in detergent solution (*20*). However, EPR studies using the 2:2 complex formed in the lipid membrane showed that the light-induced change in an interspin distance between the spin-labeled V78 residues located in the interface of two *p*HtrIIs occurred at a rate of 3 ms (*15*), which is in conflict with the data obtained by the transient grating method but not with the present data obtained in the 1:1 *p*pR/*p*HtrII complex formed in detergent solution. Interestingly, however, the relaxation of the light-induced distance change between V78 residues in a *p*HtrII/*p*HtrII pair in the 2:2 complex observed by EPR measurements was slower than the recovery of *p*pR to the initial state by a factor of 4, suggesting decoupling of the *p*HtrII relaxation from return of *p*pR to the initial state (*1*). The present results clearly indicate that the relaxation of the light-induced conformation of *p*HtrII in the 1:1 *p*pR/*p*HtrII complex is coupled tightly with the decay of the O state of *p*pR both in the absence and in the presence of azide. The discrepancy between the results obtained with the 2:2 complex in the lipid bilayer and the 1:1 complex in detergent solution may depend on the difference in the paired residues examined but not on the experimental technique. In the present FRET experiments, the light-induced conformational change occurring in a single pair of *p*pR and *p*HtrII was examined. On the other hand, since EPR experiments examined the relative motion of two *p*HtrIIs in the 2:2 *p*pR/*p*HtrII complex, the observed dynamic behavior reflects relative motion between a pair of 1:1 *p*pR/*p*HtrII units in the 2:2 *p*pR/*p*HtrII complex. The relaxation of the light-induced interunit conformation in the 2:2 complex may delay to that of the intraunit conformation.

CONCLUSION

By FRET experiment, the dynamics of light-induced intramolecular motion between A80 and L120 in *p*HtrII as well as intermolecular motions between each of several

residues in *p*pR and *p*HtrII in the 1:1 *p*pR/*p*HtrII complex formed in DDM micelle were determined. The loop and the second α-helix in the *p*HtrII linker move away from V185 and V58. However, the structure of the linker region in the 1:1 complex formed in detergent solution may be different from that in the 2:2 complex formed in the lipid membrane. Further studies in the lipid membrane are required. O-decay of *p*pR became faster in the 1:1 *p*pR/*p*HtrII complex formed in DDM compared with that in the absence of *p*HtrII, indicating that the dynamics of conformational change in *p*pR from the O state to initial state is modified by the formation of the complex with *p*HtrII as to be accelerated. Flash-induced FRET efficiency change showed that the relaxation of the light-induced conformation of *p*HtrII coincides with that of the O state of *p*pR in the 1:1 *p*pR/*p*HtrII complex, suggesting that return of the light-induced conformation of *p*HtrII to the initial state is tightly coupled with the conformational change from the O state to the initial state of *p*pR. Taken together with an EPR study with the 2:2 complex formed in the lipid membrane (*1*), we suppose that the light-induced conformational change of *p*HtrII is tightly coupled to that of *p*pR in each 1:1 *p*pR/*p*HtrII unit in the 2:2 complex through the M (rise) and O (decay) state of *p*pR. The tightly coupled conformational change of the 1:1 *p*pR/*p*HtrII unit induces the relative motion between the two units in the 2:2 complex, but the interunit motion occurs delay to intraunit motion of the 1:1 *p*pR/*p*HtrII unit.

ACKNOWLEDGMENT

We thank Dr. Kazumi Shimono and Dr. Yuki Sudo for technical advice especially on protein expression and purification.

REFERENCES

1. Wegener, A.-A., Klare, J. P., Engelhard, M., and Steinhoff, H.-J. (2001) Structural insights into the early steps of receptor-transducer signal transfer in archaeal phototaxis, *EMBO J. 20*, 5312−5319.
2. Gordeliy, V. I., Labahn, J., Moukhametzianov, R., Efremov, R., Granzin, J., Schlesinger, R., Büldt, G., Savopol, T., Scheidig, A. J., Klare, J. P., and Engelhard, M. (2002) Molecular basis of transmembrane signaling by sensory rhodopsin II-transducer complex, *Nature 419*, 484−487.
3. Moukhametzianov, R., Klare, J. P., Efremov, R., Baeken, C., Göppner, A., Labahn, J., Engelhard, M., Büldt, G., and Gordeliy, V. I. (2006) Development of the signal in sensory rhodopsin and its cognate transducer, *Nature 440*, 115−119.
4. Kim, K. K., Yokota, H., and Kim, S.-H. (1999) Four-helical-bundle structure of the cytoplasmic domain of a serine chemotaxis receptor, *Nature 400*, 787−792.
5. Budyak, I. L., Pipich, V., Mironova, O. S., Schlesinger, R., Zaccai, G., and Klein-Seetharaman, J. (2006) Shape and oligomerization state of the cytoplasmic domain of the phototaxis transducer II from *Natronobacterium pharaonis*, *Proc. Natl. Acad. Sci. U.S.A. 103*, 15428−15433.
6. Yamaguchi, S., Shimono, K., Sudo, Y., Tuzi, S., Naito, A., Kamo, N., and Saitô, H. (2004) Conformation and dynamics of the [3-^{13}C]-Ala, [1-^{13}C]Val-labeled truncated *pharaonis* transducer, *p*HtrII-(1−159), as revealed by site-directed ^{13}C solid-state NMR: changes due to association with phoborhodopsin (sensory rhodopsin II), *Biophys. J. 86*, 3131−3140.
7. Sudo, Y., Okuda, H., Yamabi, M., Fukuzaki, Y., Mishima, M., Kamo, N., and Kojima, C. (2005) Linker region of a halobacterial transducer protein interacts directly with its sensor retinal protein, *Biochemistry 44*, 6144−6152.
8. Bordignon, E., Klare, J. P., Doebber, M., Wegener, A. A., Martell, S., Engelhard, M., and Steinhoff, H.-J. (2005) Structural analysis of a HAMP domain, *J. Biol. Chem. 280*, 38767−38775.
9. Klare, J. P., Bordignon, E., Doebber, M., Fitter, J., Kriegsmann, J., Chizhov, I., Steinhoff, H.-J., and Engelhard, M. (2006) Effects of solubilization on the structure and function of the sensory rhodopsin II/transducer complex, *J. Mol. Biol. 356*, 1207−1221.
10. Yang, C.-S., Sineshchekov, O., Spudich, E. N., and Spudich, J. L. (2004) The cytoplasmic membrane-proximal domain of the HtrII transducer interacts with the E-F loop of photoactivated *Natoronomonas pharaonis* sensory rhodopsin II, *J. Biol. Chem. 279*, 42970−42976.
11. Hulko, M., Berndt, F., Gruber, M., Linder, J. U., Truffault, V., Schultz, A., Martin, J., Schultz, J. E., Lupas, A. N., and Coles, M. (2006) The HAMP domain structure implies helix rotation in transmembrane signaling, *Cell 126*, 929−940.
12. Miyazaki, M., Hirayama, J., Hayakawa, M., and Kamo, N. (1992) Flash photolysis study on *pharaonis* phoborhodopsin from a haloalkaliphilic bacterium (*Natronobacterium pharaonis*), *Biochim. Biophys. Acta 1140*, 22−29.
13. Imamoto, Y., Shichida, Y., Hirayama, J., Tomioka, H., Kamo, N., and Yoshizawa, T. (1992) Nanosecond laser photolysis of phoborhodopsin: from *Natronobacterium pharaonis* appearance of KL and L intermediates in the photocycle at room temperature, *Photochem. Photobiol. 56*, 1129−1134.
14. Chizhov, I., Schmies, G., Seidel, R., Sydor, J. R., Lüttenberg, B., and Engelhard, M. (1998) The photophobic receptor from *Natronobacterium pharaonis*: temperature and pH dependencies of the photocycle of sensory rhodopsin II, *Biophys. J. 75*, 999−1009.
15. Klare, J. P., Gordeliy, V. I., Labahn, J., Büldt, G., Steinhoff, H.-J., and Engelhard, M. (2004) The archaeal sensory rhodopsin II/transducer complex: a model for transmembrane signal transfer, *FEBS Lett. 564*, 219−224.
16. Furutani, Y., Kamada, K., Sudo, Y., Shimono, K., Kamo, N., and Kandori, K. (2005) Structural changes of the complex between *pharaonis* phoborhodopsin and its cognate transducer upon formation of the M photointermediate, *Biochemistry 44*, 2909−2915.
17. Hirai, T., and Subramaniam, S. (2003) Structural insights into the mechanism of proton pumping by bacteriorhodopsin, *FEBS Lett. 545*, 2−8.
18. Sudo, Y., and Spudich, J. L. (2006) Three strategically placed hydrogen-bonding residues convert a proton pump into a sensory receptor, *Proc. Natl. Acad. Sci. U.S.A. 103*, 16129−16134.
19. Yan, B., Takahashi, T., Johnson, R., and Spudich, J. L. (1991) Identification of signaling states of a sensory receptor by modulation of lifetimes of stimulus-induced conformations: the case of sensory rhodopsin II, *Biochemistry 30*, 10686−10692.
20. Inoue, K., Sasaki, J., Morisaki, M., Tokunaga, F., and Terazima, M. (2004) Time-resolved detection of sensory rhodopsin II-transducer interaction, *Biophys. J. 87*, 2587−2597.
21. Taniguchi, Y., Ikehara, T., Kamo, N., Watanabe, Y., Yamasaki, H., and Toyoshima, Y. (2007) Application of fluorescence resonance energy transfer (FRET) to investigation of light-induced conformational changes of the phoborhodopsin/transducer complex, *Photochem. Photobiol. 83*, 311−316.
22. Kandori, H., Shimono, K., Sudo, Y., Iwamoto, M., Shichida, Y., and Kamo, N. (2001) Structural changes of *pharaonis* phoborhodopsin upon photoisomerization of the retinal chromophore: infrared spectral comparison with bacteriorhodopsin, *Biochemistry 40*, 9238−9246.
23. Shimono, K., Iwamoto, M., Sumi, M., and Kamo, N. (1997) Functional expression of *pharaonis* phoborhodopsin in *Escherichia coli*, *FEBS Lett. 420*, 54−56.
24. Sudo, Y., Iwamoto, M., Shimono, K., and Kamo, N. (2001) *Pharaonis* phoborhodopsin binds to its cognate truncated transducer even in the presence of a detergent with a 1:1 stoichiometry, *Photochem. Photobiol. 74*, 489−494.
25. Hippler-Mreyen, S., Klare, J. P., Wegener, A. A., Seidel, R., Herrmann, C., Schmies, G., Nagal, G., Bamberg, E., and Engelhard, M. (2003) Probing the sensory rhodopsin II binding domain of its cognate transducer by calorimetry and electrophysiology, *J. Mol. Biol. 330*, 1203−1213.
26. Lackwicz, J. R. (2006) Principles of fluorescence spectroscopy, 3rd ed., Springer, New York.
27. Takao, K., Kikukawa, T., Araiso, T., and Kamo, N. (1998) Azide accelerates the decay of M-intermediate of *pharaonis* phoborhodopsin, *Biophys. Chem. 73*, 145−153.
28. Schmies, G., Lüttenberg, B., Chizhov, I., Engelhard, M., Becker, A., and Bamberg, E. (2000) Sensoryrhodopsin II from the Haloalkaliphilic *Natronobacterium pharaonis*: light-activated proton transfer reactions, *Biophys. J. 78*, 967−976.

29. Sudo, Y., Iwamoto, M., Shimono, K., and Kamo, N. (2002) Association of of *pharaonis* phoborhodopsin with its cognate transducer decreases the photo-dependent reactivity by water-soluble reagents of azide and hydroxylamine, *Biochim. Biophys. Acta 1558*, 63−69.

30. Sudo, Y., Yamabi, M., Kato, S., Hasegawa, C., Iwamoto, M., Shimono, K., and Kamo, N. (2006) Importance of specific hydrogen bonds of archaeal rhodopsin for the binding to the transducer protein, *J. Mol. Biol. 357*, 1274−1282.

31. Sudo, Y., Iwamoto, M., Shimono, K., and Kamo, N. (2002) Association between a photo-intermediate of a M-lacking mutant D75N of *pharaonis* phoborhodopsin and its cognate transducer, *J. Photochem. Photobiol. B 67*, 171−176.

32. Bergo, V. B., Spudich, E. N., Rothschild, K. J., and Spudich, J. L. (2005) Photoactivation perturbs the membrane-embedded contacts between sensory rhodopsin II and its transducer, *J. Biol. Chem. 280*, 28365−28369.

BI602482S